tion of the HDA and LDA $S(Q)$ functions. Several combinations of the $S(Q)$ of the HDA and LDA structures are plotted in Fig. 1, B (neutron data) and D (x-ray data); also plotted are the data from the sample annealed at 105 K. The annealed structures factors cannot be produced by any combination of LDA and HDA. We note the region in Fig. 1D where the x-ray curves intersect at 2.05 $Å^{-1}$, the peak is at 2.09 $Å^{-1}$ for the annealed sample, and there is only a small error in the data in this region.

The measured total structure factors of the quenched states were transformed into real-space radial distribution functions, and the several representative data sets are plotted in Fig. 4A for the neutron experiments and in Fig. 4B for the x-ray experiments. Although the neutron data are predominantly weighted toward the hydrogen–hydrogen and oxygen–hydrogen correlations and the x-ray data are predominantly weighted toward the oxygen–oxygen correlations, the major real-space structural trends upon annealing can be seen in both sets of data, and they are generally described by short- to intermediate-range structural changes between 4 and 8 Å. The broad peak centered on ~6.4 Å shifts systematically to greater distance with increasing anneal temperature. In addition, a substantial increase in the intensity of the broad peak centered at ~4.5 Å with increasing anneal temperature is noted. The hydrogen-bonded oxygen–oxygen distance, given by the position of the first peak in the x-ray $G(r)$, shortens systematically through the transformation between each amorphous form and ranges from 2.80 Å in the unannealed HDA phase to 2.76 Å in the final lowest density phase; this is consistent with measured Raman data (*23*).

We annealed HDA ice at several temperatures below 113.4 K (i.e., the recorded transition temperature to the LDA form). It is seen from the position of the FSDP in the static structure factor that the transition from the HDA form to the LDA form can proceed in a structurally continuous manner through a series of intermediate, apparently metastable amorphous forms. Several of these metastable forms were observed, and detailed radial distribution functions were compared at temperature $T = 40$ K. It is reasonable to expect that, in principle, a continuous distribution of recoverable forms between HDA and LDA ice is possible. At any $T < 113.4$ K, the thermal energy is insufficient to overcome the potential barriers that define a particular metastable structure. This is what is in general expected for the existence of any metastable phase and indicates that the transformation between the poly-amorphs of ice may be somewhat complex. From the radial distributions functions presented here, it appears that the transition predominantly evolves on the short to intermediate length scale; that is, major structural changes occur between 4 and 8 Å, and more subtle changes also occur on the hydrogen bond length scale. These data may have important implications regarding the current understanding of the structural relation between a low-density liquid water and LDA ice, and a high-density liquid water and HDA ice (*2*, *23–25*). These results may also impact on the character of the transformation from ice Ih to HDA (*5*, *26*), the HDA-LDA mixture model (*5*), and the relations between normal water and HDA. In addition, understanding structural variations in amorphous water, particularly the predominant length scales over which such variations occur, may provide a basis for understanding biomolecular hydration and cryopreservation.

References and Notes

1. O. Mishima, L. D. Calvert, E. Whalley, *Nature* **310**, 393 (1984).
2. E. F. Burton, W. F. Oliver, *Proc. R. Soc. London Ser. A* **153**, 166 (1936).
3. E. Mayer, *J. Appl. Phys.* **58**, 663 (1985).
4. O. Mishima, *J. Chem. Phys.* **100**, 5910 (1994).
5. ———, H. E. Stanley, *Nature* **396**, 329 (1998).
6. E. Whalley, O. Mishima, Y. P. Handa, D. D. Klug, *Ann. N.Y. Acad. Sci.* **484**, 81 (1986).
7. H. Schober *et al.*, *Physica B* **241–243**, 897 (1998).
8. G. P. Johari, A. Hallbrucker, E. Mayer, *Science* **273**, 90 (1996).
9. T. Loerting, C. Salzmann, I. Kohl, E. Mayer, A. Hallbruker, *Phys. Chem. Chem. Phys.* **3**, 5355 (2001).
10. O. Mishima, *Nature* **384**, 546 (1996).
11. Y. P. Handa, O. Mishima, E. Whalley, *J. Chem. Phys.* **84**, 2766 (1986).
12. C. A. Tulk, D. D. Klug, R. Branderhorst, P. Sharpe, J. A. Ripmeester, *J. Chem. Phys.* **109**, 8478 (1998).
13. E. Mayer, *J. Phys. Chem.* **89**, 3474 (1985).
14. M. A. Floriano, E. Whalley, E. Svensson, V. F. Sears, *Phys. Rev. Lett.* **57**, 3062 (1986).
15. A. Bizid, L. Bosio, A. Defrain, M. Oumezzine, *J. Chem. Phys.* **87**, 2225 (1987).
16. M. C. Bellissent-Funel, J. Teixeira, L. Bosio, *J. Chem. Phys.* **87**, 2231 (1987).
17. M. C. Bellissent-Funel, L. Bosio, A. Hallbruker, E. Mayer, R. Sridi-Dorbez, *J. Chem. Phys.* **97**, 1282 (1992).
18. L. Bosio, G. P. Johari, J. Teixeira, *Phys. Rev. Lett.* **56**, 460 (1986).
19. J. L. Finney, A. Hallbrucker, I. Kohl, A. K. Soper, D. T. Bowron, *Phys. Rev. Lett.* **88**, 225503 (2002).
20. U. Rütt *et al.*, *Nucl. Instrum. Methods A* **467**, 1026 (2001).
21. B. Tomberli, C. J. Benmore, P. A. Egelstaff, J. Neuefeind, V. Honlimaki, *J. Phys. Condens. Matter* **12**, 2597 (2000).
22. D. D. Klug, O. Mishima, E. Whalley, *J. Chem. Phys.* **86**, 5323 (1987).
23. M.-C. Bellissent-Funel, *Europhys. Lett.* **42**, 161 (1998).
24. F. W. Starr, M.-C. Bellissent-Funel, H. E. Stanley, *Phys. Rev. E* **60**, 1084 (1999).
25. A. K. Soper, M. A. Ricci, *Phys. Rev. Lett.* **84**, 2881 (2000).
26. J. S. Tse *et al.*, *Nature* **400**, 647 (1999).

27. Supported by the U.S. DOE contract nos. DE-A05-00R22725 and W-31-109-ENG-38.

20 May 2002; accepted 11 July 2002

The Vibration-Rotation Emission Spectrum of Free BeH_2

Peter F. Bernath,[1]* Alireza Shayesteh,[1] Keith Tereszchuk,[1] Reginald Colin[2]

The gaseous BeH_2 molecule has been synthesized by means of an electrical discharge inside a high-temperature furnace and identified with infrared emission spectroscopy. The antisymmetric stretching mode ν_3 has been detected near 2179 reciprocal centimeters. The BeH_2 molecule has a linear, symmetric structure with an r_0 BeH bond length of 1.333761(2) angstroms.

With only six electrons, BeH_2 is a favorite target molecule for testing new ab initio quantum chemical methods [for example, (*1–4*)]. Despite this strong interest in BeH_2, the free molecule remains unknown. It has been detected previously through its infrared spectrum when stabilized in an argon matrix at 10 K (*5*), or in a silicon crystal as an impurity (*6*). Although solid BeH_2 is well known (*7*), this material is in fact based on a three-dimensional arrangement of connected BeH_4 tetrahedra (*8*). Heating BeH_2 solid results in decomposition to the elements, not the production of BeH_2 vapor. The insertion of ground-state Be atoms into the H_2 bond is predicted (*9*) to have an activation barrier of 203.5 kJ/mol (48.6 kcal/mol), whereas the overall reaction

$$Be(g) + H_2(g) \rightarrow BeH_2(g)$$

is predicted (*10*) to be favorable and to be exoergic by 157.3 kJ/mol (37.6 kcal/mol). BeH_2 is calculated (*11*) to be linear and to have a bond length of 1.3324 Å, close to the observed value of 1.3417 Å for the BeH free radical (*12*).

We now report the formation of BeH_2 with an emission source that allows an electrical discharge inside a high-temperature furnace and the characterization of BeH_2 by infrared (IR) emission spectroscopy (*13*). The central part of

[1]Department of Chemistry, University of Waterloo, Waterloo, Ontario N2L 3G1, Canada. [2]Laboratoire de Chimie Physique Moléculaire, Université Libre de Bruxelles, C.P. 160/09, 50 avenue F. D. Roosevelt, 1050 Brussels, Belgium.

*To whom correspondence should be addressed. E-mail: bernath@uwaterloo.ca

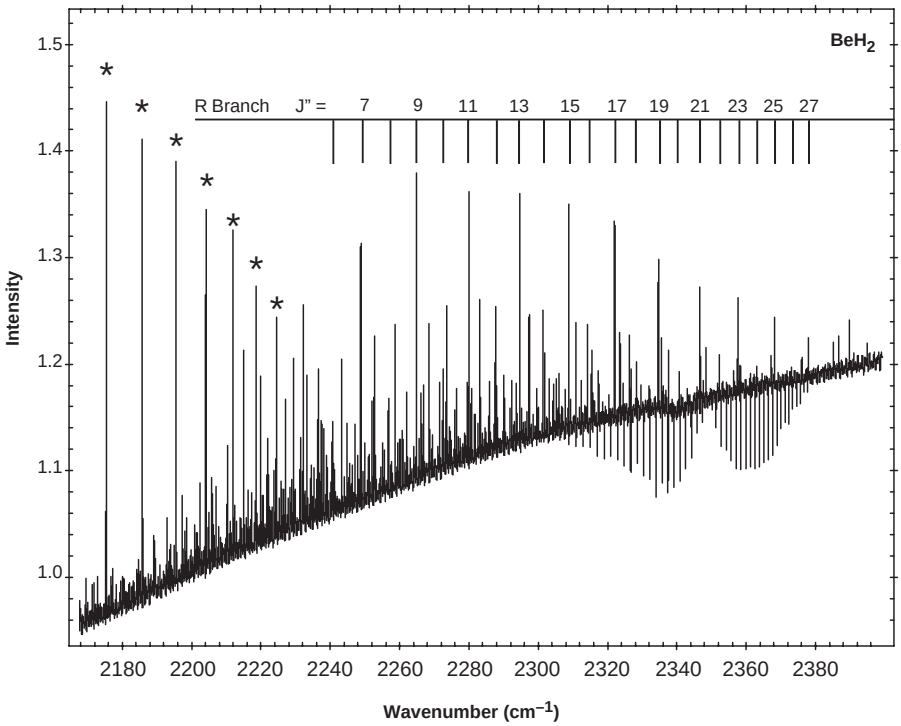

Fig. 1. A portion of the infrared emission spectrum of BeH_2. The R-branch of the antisymmetric stretching mode ν_3 is indicated. The lines of the $v = 1 \rightarrow 0$ fundamental band of BeH are marked with asterisks. The absorption of atmospheric CO_2, as well as many unassigned emission lines presumably from BeH_2 hot bands, can be seen.

an alumina tube 5 cm (outside diameter) by 120 cm long was heated to 1500°C by a CM Rapid Temp furnace. The water-cooled ends of the tube were sealed with CaF_2 windows. A slow flow of helium (about 20 torr) and hydrogen (about 10 torr) was passed through the cell. A dc discharge (2.5 kV, 333 mA) was struck between stainless-steel tube electrodes inside the alumina tube but outside the hot zone. Powdered Be metal (5 g) was placed inside a small zirconia boat in the center of the hot zone. The emission from the furnace was focused with a CaF_2 lens into the entrance aperture of a Bruker IFS 120 HR Fourier transform spectrometer. One hundred scans were recorded at a resolution of 0.03 cm^{-1} with a liquid N_2-cooled InSb detector. The spectral region was limited to 1800 to 2900 cm^{-1} by the detector response and a longwave-pass filter.

The IR emission spectra contain numerous atomic and molecular emission lines, as well as atmospheric absorption features from CO_2 and H_2O (Fig. 1). The strongest emission lines are due to the BeH free radical (*14*), for which the R-head of the $v = 1 \rightarrow 0$ fundamental band can be seen (asterisks) at the left side of the figure. In addition, a series of lines spaced by about 8 cm^{-1} with alternating 3:1 intensities can be distinguished in the figure [see table S1 for a complete list of line assignments (*15*)]. The lines listed in table S1 have an accuracy of better than 0.001 cm^{-1} based on a calibration with the BeH lines, which had been calibrated with CO in a previous spectrum (*14*). A fit of these lines to the customary rotational energy level expression (*16*), $E = \tilde{\nu} + BJ(J + 1) - D[J(J + 1)]^2 + H[J(J + 1)]^3$, results in the spectroscopic constants shown in Table 1.

The lines are assigned to the ν_3 (σ_u) antisymmetric stretching mode of the linear BeH_2 molecule for several reasons:

1) The 3:1 intensity ratio of adjacent lines is due to the ortho-para nuclear spin statistical weights associated with the nuclear spin I = ½ H nuclei (*17*). This intensity alternation is consistent with a linear, symmetric structure ($D_{\infty h}$ symmetry).

2) The gas-phase band origin of 2178.859 cm^{-1} matches the Ar matrix value of 2159 cm^{-1} (*5*), if a matrix shift is taken into account.

3) Martin and Lee's (*11*) high-level ab initio calculation of the quartic force field predicts a band origin of 2167 cm^{-1} for ν_3 as well as $B'' = 4.660$ cm^{-1} for the lower state, $B' = 4.590$ cm^{-1} for the upper state, and D_e of 1.0×10^{-4} cm^{-1}, all in good agreement with the values presented in Table 1. The predicted α_3 value of 0.070 cm^{-1}, in particular, agrees very well with the observed $B'' - B'$ value of 0.069 cm^{-1}.

The B″ value shown in Table 1 implies an r_0 bond length of 1.333761(2) Å, close to the r_e equilibrium bond length value of 1.3417 Å for BeH (*12*). The unpaired electron in the BeH free radical is in a nonbonding sp hybrid orbital, so the formation of a second bond with an H atom changes the bond length only slightly. The best ab initio value for r_0 is 1.3397 Å (*11*), and the corresponding r_e value is 1.3324 Å (*11*).

Table 1. Spectroscopic constants for the ν_3 vibrational mode of BeH_2 (in cm^{-1}). One standard deviation in the last digits quoted is in parentheses. Single primes refer to the upper state and double primes to the lower state.

Constant	Value
$\tilde{\nu}$	2178.86560(24)
B′	4.632178(13)
D′	$1.03286(36) \times 10^{-4}$
H′	$2.615(21) \times 10^{-9}$
B″	4.701380(13)
D″	$1.04942(34) \times 10^{-4}$
H″	$2.677(20) \times 10^{-9}$

Information about the other vibrational modes of BeH_2 can be deduced from the line positions of the ν_3 mode. There is a small perturbation in the $J' = 22$ energy level [the observed minus calculated values are 0.025 cm^{-1} for the R(21) and P(23) lines as compared with the typical values of <0.001 cm^{-1} (*15*)] that is likely due to an interaction with the $3\nu_2$ (π_u) vibrational level. This perturbation also confirms our rotational numbering for the ν_3 band. Our spectra still contain a number of unassigned lines (Fig. 1), many of which we expect are BeH_2 hot bands. A complete assignment currently in progress should ultimately allow an equilibrium molecular structure to be derived.

References and Notes

1. P. G. Szalay, R. J. Bartlett, *J. Chem. Phys.* **103**, 3600 (1995).
2. U. S. Mahapatra, B. Datta, D. Mukherjee, *J. Chem. Phys.* **110**, 6171 (1999).
3. D. A. Mazziotti, *Phys. Rev. A* **60**, 4396 (1999).
4. R. Baer, D. Neuhauser, *J. Chem. Phys.* **112**, 1679 (2000).
5. T. J. Tague Jr., L. Andrews, *J. Am. Chem. Soc.* **115**, 12111 (1993).
6. R. Mori, N. Fukata, M. Suezawa, A. Kasuya, *Physica B* **302–303**, 206 (2001).
7. N. N. Greenwood, A. Earnshaw, *Chemistry of the Elements* (Pergamon, Oxford, 1984), p. 125.
8. G. S. Smith *et al.*, *Solid State Commun.* **67**, 491 (1988).
9. J. Hinze, O. Friedrich, A. Sundermann, *Mol. Phys.* **96**, 711 (1999).
10. J. M. L. Martin, *Chem. Phys. Lett.* **273**, 98 (1997).
11. _____, T. J. Lee, *Chem. Phys. Lett.* **200**, 502 (1992).
12. C. Focsa, S. Firth, P. F. Bernath, R. Colin, *J. Chem. Phys.* **109**, 5795 (1998).
13. P. F. Bernath, *Annu. Rep. Prog. Chem. Sect. C* **96**, 177 (2000).
14. A. Shayesteh, K. Tereszchuk, P. F. Bernath, R. Colin, in preparation.
15. Supplementary material is available on *Science* Online.
16. G. Herzberg, *Electronic Spectra of Polyatomic Molecules* (Van Nostrand Reinhold, New York, 1966).
17. P. F. Bernath, *Spectra of Atoms and Molecules* (Oxford Univ. Press, New York, 1995), pp. 330–333.

18. We thank the Natural Sciences and Engineering Research Council (NSERC) of Canada for support.

Supporting Online Material

www.sciencemag.org/cgi/content/full/297/5585/1323/DC1

Table S1

31 May 2002; accepted 18 July 2002